

Review

# A Review on Thermophysical Property Assessment of Metal Oxide-Based Nanofluids: Industrial Perspectives

Surendran V. Sujith<sup>1</sup>, Hansoo Kim<sup>2,3,\*</sup> and Joonho Lee<sup>1,2,3,\*</sup> 

<sup>1</sup> Department of Materials Science and Engineering, Korea University, 145 Anam-ro, Seongbuk-gu, Seoul 02841, Korea; sujith\_sv@korea.ac.kr

<sup>2</sup> Institute for High Technology Materials and Device, Korea University, 145 Anam-ro, Seongbuk-gu, Seoul 02841, Korea

<sup>3</sup> Center for Research and Education of Metallurgy, Korea University, 145 Anam-ro, Seongbuk-gu, Seoul 02841, Korea

\* Correspondence: hansookim@korea.ac.kr (H.K.); joonholee@korea.ac.kr (J.L.)

**Abstract:** Energy consumption in the industrial sector can be significantly reduced by improving heat transfer rates in heat exchanger circuits, pool boiling, metal cutting industries, etc. Numerous energy-related issues can be overcome to a large extent by improving heat flow properties by utilizing nanofluids. The present contribution reviews the improvement in thermophysical properties of metal oxide-based nanofluids. Key parameters affecting the thermophysical properties of nanofluids, such as particle volume fraction, temperature, particle size and various stabilizers, were reviewed. The importance of DLVO theory and zeta potential to control the electrostatic repulsion and pH values of nanofluids for stable nanofluid formulations were discussed. It has been observed that classical theories of thermal conductivity and viscosity cannot predict exact values for a wide range of variables. Therefore, various extensive correlations have been introduced to predict the thermophysical properties of nanofluids. In these correlations, individual dependent variables such as particle size, temperature, nanofluid layer thickness, and Brownian velocity of nanoparticles, etc. were considered for more accurate prediction. The heat transfer efficiencies of nanofluids to base fluids in the laminar and turbulent regimes have been discussed using various figures of merits. Finally, the scope of industrial applications of metal oxide-based nanofluids and future research opportunities have been discussed.

**Keywords:** thermal conductivity; zetapotential; viscosity; specific heat; wettability; pool boiling; energy efficiency



**Citation:** Sujith, S.V.; Kim, H.; Lee, J. A Review on Thermophysical Property Assessment of Metal Oxide-Based Nanofluids: Industrial Perspectives. *Metals* **2022**, *12*, 165. <https://doi.org/10.3390/met12010165>

Academic Editor: Alexander McLean

Received: 10 December 2021

Accepted: 11 January 2022

Published: 17 January 2022

**Publisher's Note:** MDPI stays neutral with regard to jurisdictional claims in published maps and institutional affiliations.



**Copyright:** © 2022 by the authors. Licensee MDPI, Basel, Switzerland. This article is an open access article distributed under the terms and conditions of the Creative Commons Attribution (CC BY) license (<https://creativecommons.org/licenses/by/4.0/>).

## 1. Introduction

Out of the total energy harnessed directly and indirectly, 70% is produced by heat generation [1]. Therefore, heat exchange systems must be better engineered for more efficient energy consumption. The improvement of conductive and convective heat transfer is one of the most significant scientific challenges in almost every industrial sector. This can be achieved by changing flow geometry, boundary conditions, or by enhancing thermophysical properties of the fluid. It has been proven over the years that thermal fluids are responsible for minimizing energy loss in heat transfer systems [2,3]. Due to the exhaustion of natural resources and the increase in the demand for energy, it is very important to increase the energy efficiency of heat transfer devices. After many years of investigation, researchers have proved that nanofluids have the potential for improving the efficiency of heating and devices [4,5]. Traditionally, heat dissipation is augmented by increasing the surface area of the system, but this leads to an undesirable size of the thermal management system. Therefore, the innovative concept of nanofluids has attracted great attention to maintain miniaturized systems with improved efficiency. The emergence of nanofluids has improved the heat transfer in the thermal systems like solar heat collectors,

high power engines, microelectronic devices, and nuclear reactors [6]. Nanofluids are homogeneous suspensions of nanoparticles in different base fluids such as water, ethylene glycol, lubricating oils, etc. [7,8]. These nanoparticles upgrade the thermophysical properties such as viscosity, thermal conductivity, specific heat capacity (SHC), diffusivity, and density of the base fluids to a great extent. These suspended nanoparticles can be metallic, nonmetallic, metal oxides, and other compounds. Out of these, the suspensions of metal oxide nanoparticles are widely used due to their chemical stability, economy, and ease of production. Widely used metal oxide nano particles include  $\text{Al}_2\text{O}_3$ ,  $\text{SiO}_2$ ,  $\text{TiO}_2$  and  $\text{CuO}$  [9–12].

Maxwell originally proposed the theoretical model for improving the thermal conductivity of suspensions containing solid particles compared to the base liquid [13]. When the density of coarse particles is high or the average particle size is large, the suspensions lead to a lack of stability, and it finally settles down. This leads to additional flow resistance and possible erosion in the components of the system. Fluids with suspended nanometer-scaled particles (less than 100 nm) are termed as nanofluids, a term proposed by Choi in 1995 [14]. These fluids are considered as next generation heat transfer fluids. The large surface area of nano particles enhances both the stability and heat transfer within the system. It also improves the abrasion-related properties as compared to the conventional solid–liquid mixtures.

Nano particles are classified as metallic and nonmetallic according to the material type. Depending on the constituent material type, stabilizing methods of the nano particles are varied. Among various nanofluids, metal-oxide based nanofluids are most widely applicable due to their long shelf life and chemical and thermal stability [15]. In the present contribution, we try to deliver the state of the physics behind the enhancement in the stability and thermophysical properties of the metal oxide-based nanofluids. The aim of this review is to introduce the recent progress in the research on the thermophysical properties of metal oxide-based nanofluids. This includes the major thermophysical properties such as thermal conductivity, viscosity, specific heat, density, and wettability which have significant effects on the heat transfer characteristics. Also, the influence of size, shape, concentration, hydrodynamic size of the nanoparticles, pH, and stability are considered. Various mechanisms governing the thermal transport properties in the molecular level such as liquid layering over the nanoparticles, Brownian motion of the nanoparticles, and nanoparticle clustering have been discussed. We also critically review the challenges and future directions towards the applications of nanofluids, providing a solid foundation for industrial nanofluids.

## 2. Nanofluid Formulation

The initial step of nanofluid preparation is to formulate the preferred volume fractions of nanoparticles according to the mass of nanoparticles using the following expression [16]. Volume fraction is determined by

$$\phi = \left( \frac{\frac{m_{np}}{\rho_{np}}}{\frac{m_{np}}{\rho_{np}} + \frac{m_{bf}}{\rho_{bf}}} \right) \quad (1)$$

Here  $m$  and  $\rho$  are the corresponding mass and density of the base fluid ( $bf$ ) and nanoparticles ( $np$ ). The stability of the nanofluids should be ensured by controlling pH and zeta potential. Once the nano particles and base fluid are mixed, the whole suspension must be sonicated in a temperature-controlled ultra-sonication system by optimizing the frequency and amplitude of the ultrasonic waves to make stable suspensions. The whole step is shown in Figure 1.

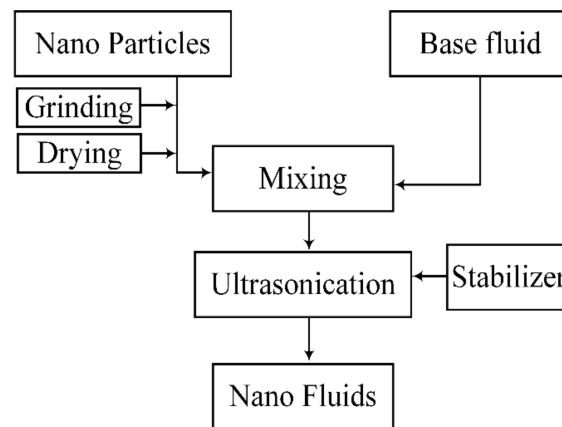


**Figure 1.** Steps involved in the nanofluid formulation process.

### 2.1. Stability Assessment

The stability of nanofluids controls the steady state functioning of the heat transfer system. The agglomeration of nanoparticles due to the strong van der Waals force leads to the reduction in the Brownian motion of the particles, significantly diminishing the heat transfer. This also distracts the flow behavior by augmenting frictional resistance. Hence, it must be ensured that the nanoparticles are dispersed uniformly in the fluid due to the electrical double layer repulsion by increasing the zeta potential to its maximum value [17].

The most critical point in the formulation of the nanofluids is the dispersion process to ensure nanoparticle suspension stability. The suspension stability is governed by the surface forces (attractive and repulsive) acting among the particles. In general, a two-step method is employed to prepare nanofluids [17,18]. Initially, nanoparticles are added into the base fluid. After that, ultra-sonication is applied to break the agglomeration of particles. Depending on the nanoparticles and base fluids, the ultrasonic power and sonication time should be optimized to obtain homogeneous dispersion and long-term stability. The sonication process must be combined with various stabilization methods such as steric or electrostatic repulsion to realize long-term stability of the nanofluids. This is achieved by using surfactants or by modifying pH [19]. Surfactants are surface active agents, which are amphipathic molecules consisting of non-polar portion attached to a polar or ionic portion. These can be cationic, anionic, or nonionic. The amphiphilic structure of surfactants adsorbs at the interfaces and modifies the properties such as surface tension, wettability and overall thermophysical properties of the system [20]. Hence, there should be a balance between the suspension stability and the effectiveness of these surfactants on the thermophysical properties of the system.

To achieve colloidal stability, electrostatic and steric electrostatic stabilization was used to modify the surface chemistry. The potential difference between the adsorbed layer on the nanoparticle and the bulk liquid is defined as zeta potential as shown in Figure 2. The pH value of a fluid must be away from the isoelectric point to make a stable nano suspension as shown in Figure 3. At the isoelectric point, the zeta potential of the particle becomes zero, which maximizes the attraction between particles. To make a stable nano suspension, the pH value should be shifted in such a way that the electrical charge density of the particles should promote repulsive forces between them. Therefore, the pH value of the suspension would be modified to control the surface potential of nanoparticles reflected by zeta potential. The pH value can be controlled by adding various buffer solutions. Their compatibility within the suspension must be ensured. This is called electrostatic stabilization [21]. In the case of electro steric stabilization, surfactants are added into the solution. The surfactants dissociate into ions and adsorb on the particle surface, providing higher surface charge to the particles. This surface charge of the particle is called zeta potential. Hydrodynamic size distribution (HSD),  $D_z$  provides the effective size of the

nanoparticles at which the solvent molecules attached to them [22]. HSD is calculated by the intensity weight distribution curve given below.

$$D_z = \frac{\sum S_i}{\sum \left(\frac{S_i}{D_i}\right)} \tag{2}$$

where  $S_i$  is the scattered light intensity of  $i$ th particle and  $D_i$  is the diameter of  $i$ th particle. Zeta potential and HSD can be analyzed by using a zeta potential analyzer. The criterion for a stable suspension is a zeta potential value of  $-30$  or  $+30$  mV over time [23]. This surface charge overcomes the attractive van der Waals forces between the particles.

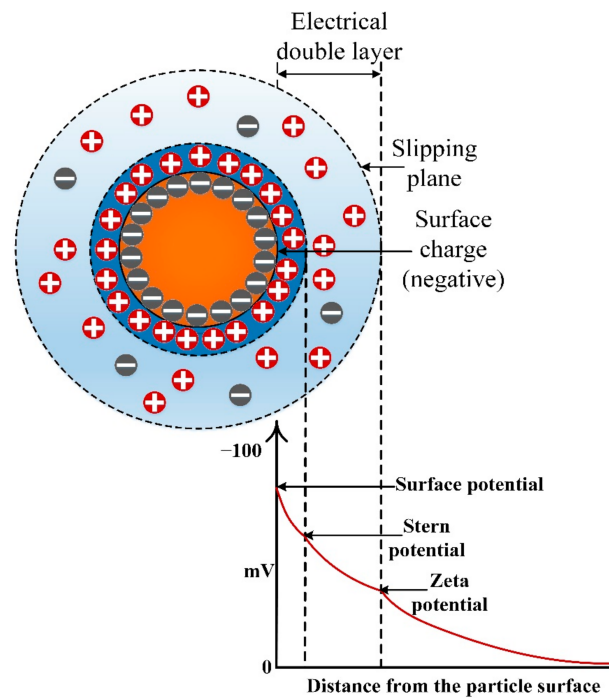


Figure 2. Schematic illustration of electrical double layer and zeta potential.

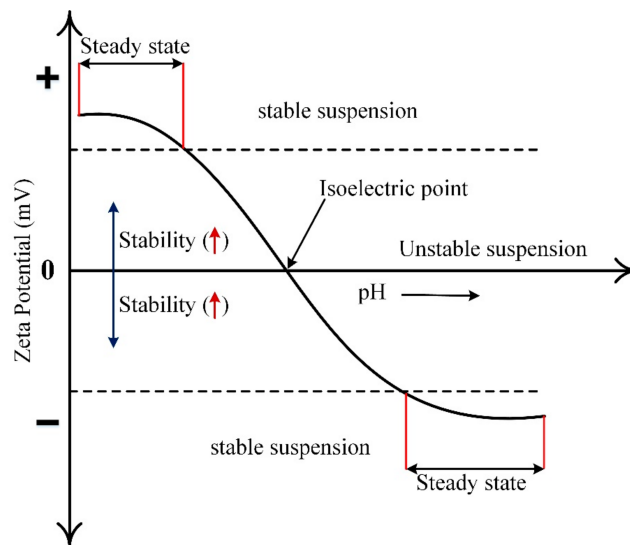


Figure 3. Schematic illustration of a zeta potential vs. pH curve showing the isoelectric point which determines the degree of a nanofluid’s stability.

## 2.2. DLVO Theory and Its Significance

The stability of lyophobic colloids is explained by the theory developed by Derjaguin, Landau, Verwey, and Overbeek (DLVO). [24]. DLVO theory describes the interaction of the local electric field developing around the particles in an aqueous medium. It explains the effect of the van der Waals force ( $\psi_A$ ) and electrostatic repulsive force ( $\psi_R$ ) between a pair of particles as a function of the distance between them ( $H$ ). The combination of two forces provides the net interaction energy as shown in Figure 4. Natures of particles and aqueous medium govern the net interaction energy. If two particles possess enough kinetic energy to overcome the maximum repulsive force (energy barrier), they will agglomerate, resulting in an unstable suspension [25]. The total interaction energy,  $\psi_T$ , is a function of the shortest distance between the particle surfaces ( $H$ ).

$$\psi_T = \psi_R + \psi_A \quad (3)$$

For a surface potential ( $\psi_o$ ) of nano particles, the electrostatic repulsive energy ( $\psi_R$ ) is given as follows.

$$\psi_R = 2\pi\epsilon a\psi_o^2 \ln [1 + e^{(-kH)}] \quad (4)$$

where  $\epsilon$  is the dielectric permittivity of the solvent,  $\kappa^{-1}$  is the thickness of electrical double layer (EDL) or Debye's length, and  $a$  is the particle radius. The simplified van der Waals attractive energy for spherical particles at close separations ( $H \ll a$ ) is given as follows.

$$\psi_A(H) = -\frac{aA}{12H} \quad (5)$$

where  $A$  is Hamaker's constant, which depends on the particle properties and the dispersing medium.

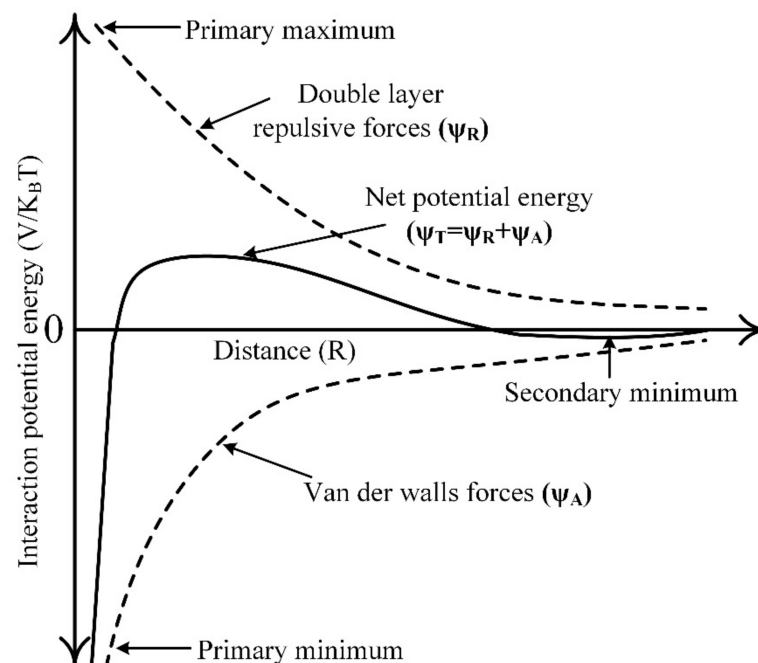


**Figure 4.** Potential energy interaction as a function of inter-molecular distance.

Zeta potential ( $ZP$ ) is calculated indirectly from the Henry's equation of electric field which is given below [26].

$$\frac{U}{E} = \frac{2\epsilon\zeta}{3\mu} f(\kappa a) \quad (6)$$

where  $(U/E)$  is the electrophoretic mobility which is the ratio of particle velocity to the electric field strength ( $\text{m}^2 \text{s}^{-1} \text{V}^{-1}$ ),  $\zeta$  is the zeta potential (V),  $\varepsilon$  is the dielectric permittivity of solvent ( $\text{kg m V}^{-2} \text{s}^{-2}$ ),  $\mu$  is the dynamic viscosity ( $\text{kg m}^{-1} \text{s}^{-1}$ ), and  $f(\kappa a)$  is the Henry's function, which varies from 1 to 1.5.  $\kappa^{-1}$  is the thickness of electrical double layer (EDL), and  $a$  refers to the particle radius. Hence,  $\kappa a$  represents the ratio of particle radius to the thickness of EDL.

### 3. Effect of Metal-Oxide Based Nanofluids on Thermophysical Properties

#### 3.1. Specific Heat

Specific heat capacity (SHC) of a nanofluid is defined as the capability of the nanofluid to absorb heat energy without any phase change. It quantifies various essential thermal behaviors such as the rate of heat transfer, the efficiency of the heat exchanger and the average Nusselt number. Specific heat capacity is critical to the accurate design and assembly of heat transfer applications through cooling and lubrication systems, such as solar collectors, refrigeration and air conditioning, machining, etc. [23,27,28]. The governing equations below show the effect of specific heat capacity on thermal transport properties such as thermal diffusivity, thermal conductivity, density, and the efficiency of the heat exchanger, etc.

$$\alpha = \frac{k}{\rho C_p} \quad (7)$$

where  $k$ ,  $\rho$ ,  $C_p$  and  $\alpha$  denote thermal conductivity, density, specific heat capacity and thermal diffusivity, respectively. Rate of heat transfer,  $\dot{q}$ , is given by the following equation.

$$\dot{q} = \dot{m} C_p \Delta T \quad (8)$$

where  $\dot{m}$  and  $\Delta T$  represent mass flow rate and temperature difference, respectively [27]. For example, the effectiveness of the heat exchanger system,  $\varepsilon$ , is given by the following equation.

$$\varepsilon = \frac{1 - e^{(-NTU \cdot (1 - C_r))}}{1 - C_r e^{(-NTU \cdot (1 - C_r))}} \quad (9)$$

$$C_r = \frac{C_{min}}{C_{max}} C = \dot{m} C_p, \quad NTU = \frac{UA}{C_{min}} \quad (10)$$

where  $NTU$ ,  $C_{min}$ ,  $C_{max}$ ,  $U$  and  $A$  are the number of transfer units, minimum heat capacity rate, maximum heat capacity rate, overall heat transfer coefficient and heat transfer area, respectively.

The experimentally developed local heat transfer coefficients are generally validated by the Dittus–Boelter correlation, which is given below [28].

$$Nu = 0.023 \times Re^{0.8} \times Pr^{0.4} \quad (11)$$

$$Pr = \frac{C_p \mu}{k} \quad (12)$$

where  $Nu$ ,  $Re$  and  $Pr$  are Nusselt, Reynolds and Prandtl numbers, respectively.

Table 1 lists a few models and correlations for the calculation of SHC of nanofluids available from various literature with respect to intensive experimentation. Pak and Cho [29] developed a mixing model for the turbulent friction and heat transfer behavior of metal oxide-based nanofluids. Vajjiha and Das [30] reported the specific heat measurement of three nanofluids containing ZnO, Al<sub>2</sub>O<sub>3</sub>, and SiO<sub>2</sub> nanoparticles in the aqueous solution of 40 wt.% ethylene glycol. The experimental data were not in close agreement with the existing correlations; hence a new correlation for specific heat as a function of temperature, volume fraction of particles, and specific heat of the base fluid was developed and predicted with an average error of 2.7%. Zhou et al. [31] investigated the specific heat capacity of CuO nanoparticles with ethylene glycol as the base fluid. As the difference in density between the base fluid and nanoparticles is large, a new correlation has been

developed taking into account both the density of the base fluid and nanoparticles. After reviewing more than 80 experimental data on water-based Al<sub>2</sub>O<sub>3</sub> nanoparticles, Sekhar and Sharma [32] developed a novel correlation by regression involving the effect of temperature and nanoparticle diameter. The below mentioned are the major theoretical models for calculating the specific heat of metal oxide-based nanofluids with good accuracy.

**Table 1.** Specific heat capacity estimation of metal oxide-based nanofluids (model and correlations).

Models/Correlations	Author
$C_p^{nf} = \phi C_p^{np} + (1 - \phi) C_p^{bf}$	Pak and Cho [29]
$\frac{C_p^{nf}}{C_p^{bf}} = \frac{\left[ \left( A \times T + \left( B \times \frac{C_p^{np}}{C_p^{bf}} \right) \right) \right]}{C + \phi}$ A, B and C are correlation coefficients	Vajjha and Das [30]
$C_p^{nf} = \frac{\rho_{np} \phi_{np} C_p^{np} + (1 - \phi) \rho_{bf} C_p^{bf}}{\phi C_p^{np} + (1 - \phi) \rho_{bf}}$	Zhou et al. [31]
$C_p^{nf} = 0.8429 \left( 1 + \frac{T_{nf}}{50} \right)^{-0.3037} \times \left( 1 + \frac{d_p}{50} \right)^{0.4167} \times \left( 1 + \frac{\phi}{100} \right)^{2.272}$	Shekar and Sharma [32]
$C_p^{nf} = \frac{\rho_{np} \phi_{np} C_{p, np} + \rho_s \phi_s C_{p, s} + \rho_{ns} \phi_{ns} C_{p, ns}}{\rho_{np} \phi_{np} + \rho_s \phi_s + \rho_{ns} \phi_{ns}}$	Donghyun and Debjyoti [33]

Mostly, the specific heat values of water and ethylene glycol-based metal oxide nanofluids containing Al<sub>2</sub>O<sub>3</sub>, SiO<sub>2</sub>, CuO, TiO<sub>2</sub>, and ZnO decreased with the increase in the nanoparticle concentrations [34–36]. Shin et al. [37] synthesized the nanofluids by dispersing Al<sub>2</sub>O<sub>3</sub> particles with a size of 1 nm in an alkali eutectic salt. The eutectic composition of potassium carbonate and lithium carbonate (molar ratio 38:62) was dissolved in water at a concentration of 1.0% by weight. They observed the formation of ordered chain-like nanostructures inside the suspension. When Al<sub>2</sub>O<sub>3</sub> nanoparticles are suspended in the water, Al(OH)<sub>3</sub> is formed on the surface, with a surface charge of (OH<sup>-</sup>). When Al<sub>2</sub>O<sub>3</sub> nanoparticles are dispersed in the eutectic salt of Li<sub>2</sub>CO<sub>3</sub> and K<sub>2</sub>CO<sub>3</sub>, the charged nanoparticles interact with Li<sup>+</sup> and K<sup>+</sup>. The nucleation and growth of crystal salt structures form an interconnected percolating network within the suspension, thereby increasing the specific surface area of the nanoparticles and improving the specific heat capacity of the nanofluid. TEM images of fractal-like fluid nanostructure formation and related mechanisms are shown in Figure 5a,b. This is because water and ethylene glycol have higher specific heat values compared to the effective specific heat values of nanoparticles. Many studies have reported that the specific heat capacity of salt-based nanofluids is similarly improved by the increase in specific surface area compared to conventional nanofluids. [38–41]. Quinbo et al. [40] investigated the effectiveness of TiO<sub>2</sub> nanoparticles in BaCl<sub>2</sub>-H<sub>2</sub>O solution exhibiting a phase transition at a temperature of −8 °C and pH 8. The pH was maintained using HCl and NaOH. The main purpose of their research was to use this fluid as a refrigerant for cold storage due to its low phase change temperature of −8 °C. The maximum decrease in specific heat was observed between 10 °C and 80 °C to 3.1% for the nanoparticles at 1.1 vol%. Gaio et al. [42] Performed both simulation and experimental study of the specific heat capacity of molten salt based nanofluids. Molecular dynamics studies have been employed by considering energy fluctuations inside molten salts due to the addition of SiO<sub>2</sub> nanoparticles inside sodium nitrite, lithium nitrite and potassium nitrite. The specific heat values were experimentally investigated and validated using simulation and thermal equilibrium model.

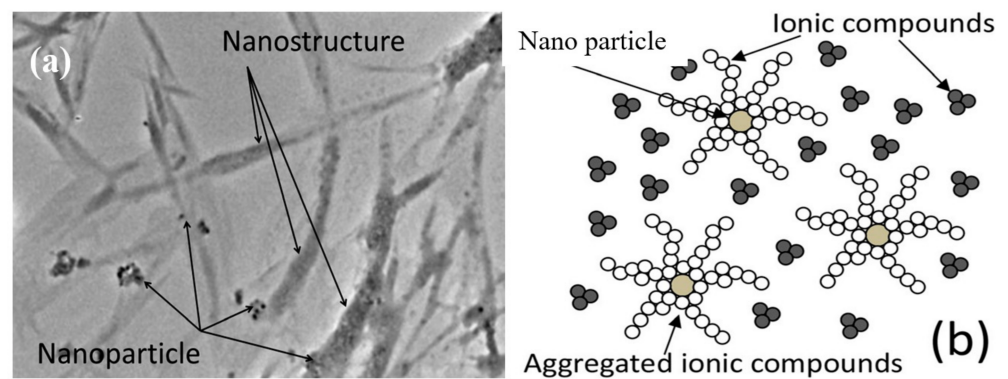


**Figure 5.** Nanostructures are grown from each nanoparticle and connect each other to form fractal-like fluid nanostructures. (a) TEM image of fractal-like fluid nanostructures formed in a molten salt nanofluids by separated base molten salts; (b) corresponding schematic illustration [37].

### 3.2. Thermal Conductivity

Over the years, several studies have been conducted on the thermal conductivity of nanofluids, and various theoretical and numerical models have been proposed. Classical models based on mixture and compound theory include those of Maxwell [13], Hamilton crosser [43], Bruggemen [44], Yamada, and Ota [45]. For example, Sujith et al. [46] experimentally investigated the thermal conductivity of pure coconut oil-based  $\text{Al}_2\text{O}_3$  nanofluids, and the results obtained from Maxwell's and Yamada's models differed from experimental data by 22 and 28%, respectively. This is because these models considered only the conventional factors such as particle type, volume fraction, and base fluid type. Researchers also found many other simultaneous factors affecting the thermal conductivity of the nanosuspensions. Therefore, new mathematical models and empirical correlations were proposed by considering Brownian motion of the nanoparticles, nano-layering of the base fluid at liquid/nanoparticle interface, temperature of the base fluid, diameter of the nanoparticles and nanoparticle clustering [47]. Table 2 shows the selected models and correlations widely used for thermal conductivity evaluation of metal oxide-based nanofluids.

Hwang et al. [48] investigated the thermal conductivities of  $\text{TiO}_2$  (25 nm),  $\text{Al}_2\text{O}_3$  (48 nm), Fe (10 nm), and  $\text{WO}_3$  (38 nm) nano-suspensions and compared them with each other. Ethylene glycol and deionized water were used as the base fluid in their study. The nanoparticles were synthesized by the chemical vapor deposition route in their study. They concluded that the specific surface area of nanoparticles is a major factor in determining the thermal conductivity of nanofluids. Hemmat et al. [49] experimentally analyzed the thermal conductivity of hybrid nanofluids containing MWCNT-MgO/water-EG nanofluids. Their tests were performed at temperatures ranging from 30 to 500 °C at a solid volume fraction of 0.015 to 0.96%. In addition, price–performance analysis was performed according to industrial needs in terms of performance and efficiency. They concluded that hybrid nanofluids outperform single particle nanosuspensions.

**Table 2.** Thermal conductivity estimation of metal oxide-based nanofluids (model and correlations).

Models/Correlations	Author
$k_{nf} = k_{bf} \frac{k_{np} + 2k_{bf} + 2\phi(k_{np} - k_{bf})}{k_{np} + 2k_{bf} - \phi(k_{np} - k_{bf})}$	Maxwell [13]
$\phi \left[ \frac{k_{np} - k_{nf}}{k_{np} + 2k_{nf}} \right] + (1 - \phi) \left[ \frac{k_{bf} - k_{nf}}{k_{bf} + 2k_{nf}} \right] = 0$	Burggeman [44]
$k_{nf} = k_{bf} (1 + 3\phi)$	Timoofeva [50]
$k_{nf} = \left[ 1.271 Re^{-0.206} Pr^{0.372} \left( \frac{T}{T_{fr}} \right)^{0.372} \left( \frac{k_p}{k_{bf}} \right)^{-0.328} \phi^{0.0076} \right] k_{bf}$	Sujith et al. [46]
$k_{nf} = \frac{\frac{k_p}{k_{bf}} + \psi + \psi \phi \left( 1 - \frac{k_p}{k_{bf}} \right)}{\frac{k_p}{k_{bf}} + \psi + \phi \left( 1 - \frac{k_p}{k_{bf}} \right)}$ $\psi = 2\phi^{0.2} \left( \frac{d_p}{d_p} \right)$ for cylindrical particles, $\psi = 2\phi^{0.2}$ for spherical particles	You and Choi [47]
$k_{nf} = \left[ \frac{k_p + (n-1)k_{bf} - (n-1)(k_{bf} - k_p)\phi_p}{k_p + (n-1)k_{bf} + (k_{bf} - k_p)\phi_p} \right] k_{bf}$ , $n = 3/\psi$	Hamilton-crosser [43]
$k_{nf} = k_{static} + k_{Brownian}$ $k_{static} = k_{bf} \left[ \frac{k_{np} + 2k_{bf} + 2\phi(k_{np} - k_{bf})}{k_{np} + 2k_{bf} - \phi(k_{np} - k_{bf})} \right]$ $k_{Brownian} = 5 \times 10^4 \beta \phi \rho_{bf} C_p^{bf} \sqrt{\frac{k_B T}{\rho_{np} d_{np}}} f$	Koo and Kleinstreuer [51]
$\frac{k_{nf}}{k_{bf}} = 1.268 \left( \frac{T}{80} \right)^{-0.0074} \times \left( \frac{\phi}{100} \right)^{0.036}$	Sadik et al. [52]
$k_{nf} = \left( 1 + a\phi_p + b\phi_p^2 \right) k_{bf}$	Liu and Lin [53]

### 3.3. Viscosity

The study of a fluid’s response to the applied shear stress is called rheology [54]. Shear stress versus shear rate gives the rheological behavior of a particular fluid. The ratio of shear stress and strain rate is termed as viscosity, and this determines the rheological properties of a fluid. In general, fluids are categorized into Newtonian and non-Newtonian types. Newtonian fluids exhibit a linear relation between the shear rate and shear stress. While non-Newtonian fluids show a nonlinear relationship, and the fluid flow curve does not intersect the center of the axes of the coordinate system [55]. Figure 6 shows the difference in the fluid flow curves of Newtonian and non-Newtonian fluids. Viscosity is one of the most critical factors determining the stability of a fluid especially in high temperature applications. It also determines the interfacial friction between the fluid layers. To analyze the pumping power requirement in various thermal applications, the rheological behavior of fluid flow must be considered. Many experimental reports showed that the increase in the nanoparticle concentration improved the viscosity of metal oxide-based nanofluids [56,57]. This is because the internal friction between the fluid layers increases with the increase in the viscosity. Table 3 presents the relative viscosity of metal oxide-based nanofluids at several different temperatures.

**Table 3.** Relative viscosity of various metal oxide based nanofluids at several different temperatures.

Author	Nanoparticles	Base Fluid	Temperature-Range (°C)	Relative Viscosity (Maximum)
Xichen et al. [58]	Al <sub>2</sub> O <sub>3</sub>	Engine oil (SN 5W–40)	Ambient	1.12
Mostafizur et al. [59]	TiO <sub>2</sub>	Methanol	1–20	1.65
Chiam et al. [60]	Al <sub>2</sub> O <sub>3</sub>	60:40 (W:EG)	30–70	1.67
Fedele et al. [61]	TiO <sub>2</sub>	Bidistilled water	10–70	2.8
Sujith et al. [9]	Al <sub>2</sub> O <sub>3</sub>	Coconut oil	30–140	2.5
Georgiana et al. [62]	Al <sub>2</sub> O <sub>3</sub> /SiO <sub>2</sub>	Distilled water	Ambient	2.7
Suhaib et al. [63]	ZnO	Paraffin oil	25–55	1.62
Yan et al. [64]	TiO <sub>2</sub> /MWCNT	Ethylene glycol	25–55	1.94
Kole et al. [65]	CuO	Gearoil	10–80	2.8
Andac et al. [66]	ZrO <sub>2</sub>	Water	10–70	1.8
Sonawane [67]	Fe <sub>3</sub> O <sub>4</sub>	Ethylene glycol	20–80	2.18

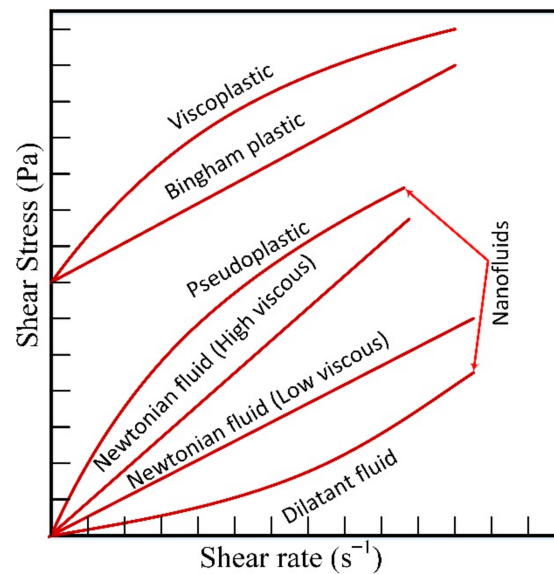


**Figure 6.** Various rheological behaviors of different fluids.

Xichen et al. [58] experimentally investigated the effect of nanoparticle size on the viscosity of nanofluids. Two types of nanoparticles ( $\text{Al}_2\text{O}_3$  and  $\text{ZnO}$ ) were added to engine oil with varying particle sizes from 20 nm to 100 nm with solid volume fractions ranging from 1% to 5%. The viscosity of the nanofluids increased as the particle concentration of both nanofluids increased. Based on the DLVO theory, they conclude that the interparticle spacing and the degree of particle agglomeration are the main mechanisms involved in improving the viscosity of nanofluids. Mostafizur et al. [62] observed the rheological behavior of Methanol- $\text{Al}_2\text{O}_3$  and Methanol- $\text{TiO}_2$  nanofluids at different shear rates and temperatures. The viscosity and shear stress of nanofluids increased with increasing shear rate. The highest viscosity increase of 64% compared to the base fluid was obtained at 0.15%  $\text{TiO}_2$  among the  $\text{TiO}_2$ -methanol nanofluids. Aminan et al. [63] proposed a feed-forward ANN model to accurately estimate the kinematic viscosities of different nanofluids over a wide range of particle concentrations and temperatures. Numerous experimental data from the available literature were collected for eight different nanofluids ( $\text{Fe}_3\text{O}_4$ -water, Ni-water, Ag-water,  $\text{Al}_2\text{O}_3$ -water, CuO-water,  $\text{TiO}_2$ -water, MWCNT-water, SiC-water) with particle diameters ranging from 7 nm to 100 nm. The absolute mean deviation of the proposed ANN model for all nanofluids was about 6.6% and the  $R^2$  value was 0.9842.

Several studies have attempted to correlate the viscosity of nanofluids by comparing experimental data with classical models. One of the well-known classical models is Einstein's viscosity equation, developed in 1906, which allows a linear estimate of viscosity by considering only the volume fraction of nanoparticles suspended in solution [68]. Many researchers have found that this is only valid for low volume fractions of less than 0.2%. Brinkman [69] improved the accuracy of the Einstein model for higher volume fractions up to 0.4%. Lundergan [70] proposed a relationship based on Taylor expansion series. Subsequently, Krieger and Dougherty [54] further proposed a semi-empirical power law model for spherical suspensions with a maximum volume fraction of 0.6%. Bachelor [71] also improved the Einstein model by considering the influence of Brownian motion and the thermal properties of nanoparticles. Later, Wang et al. [72] also proposed a relationship similar to Bachelor's model. Table 4 shows the models and correlations widely used for the evaluation of the kinematic viscosity of metal oxide-based nanofluids.

**Table 4.** Viscosity estimation of metal oxide based nanofluids (Model and correlations).

Models/Correlations	Author
$\frac{\mu_{nf}}{\mu_{bf}} = 1 + 2.5\phi$	Einstein [68]
$\frac{\mu_{nf}}{\mu_{bf}} = (1 - \phi)^{-2.5}$	Brinkman [69]
$\frac{\mu_{nf}}{\mu_{bf}} = 1 + 2.5\phi + 6.5\phi^2$	Batchelor [71]
$\frac{\mu_{nf}}{\mu_{bf}} = 1 + 7.3\phi + 123\phi^2$	Wang [72]
$\frac{\mu_{nf}}{\mu_{bf}} = \left(1 - \frac{\phi}{\phi_m}\right)^{-[\eta]\phi_m}$ $\eta = \text{intrinsic viscosity} = 2.5$ $\phi_m = 0.605$	Krieger and Dougherty [54]
$\frac{\mu_{nf}}{\mu_{bf}} = \frac{1}{1 - 34.87(d_p/d_f)^{-0.3}\phi^{1.03}}$ $d_f = \text{equivalent diameter of the base fluid molecule}$	Massimo [73]
$\log\left(\frac{\mu_{nf}}{\mu_{bf}}\right) = Ae^{-BT}$ $A = 1.8375\phi^2 - 29.643\phi + 165.56$ $B = 4 \times 10^{-6}\phi^2 - 0.001\phi + 0.0186$	Namburu et al. [74]
$\mu_{nf} = \mu_{bf} + \rho_p V_b d_p^2 / (72N\delta)$	Masoumi et al. [75]
$\frac{\mu_{nf}}{\mu_{bf}} = (1 + 2.5\phi + 4.83\phi^2 + 6.4\phi^3)$	Christiana and Kumar [76]
$\frac{\mu_{nf}}{\mu_{bf}} = \left(1 + 2.5\phi + 4.5 \left[ \frac{1}{\left(\frac{h}{d_p} \left[2 + \frac{h}{d_p}\right]\right) \left(1 + \frac{h}{d_p}\right)^2} \right]\right)$ h is the inter particle distance	Graham [77]

### 3.4. Nucleate Boiling and Wettability

Nucleate boiling is a very important heat transfer mechanism in many industrial applications such as chemical reactors, nuclear reactors, high-power electronics, and refrigeration systems. Numerous investigations have concluded that nanoparticles improve surface wettability and enhance the critical heat flux (CHF) in pool boiling heat transfer [78–81]. The reliability of the experimentations is validated by the well-known Rohsenow correlation [82] as follows.

$$q = \mu_l h_{fg} g \sqrt{\left[ \frac{g(\rho_l - \rho_v)}{\sigma_{lv}} \right]} \left[ \frac{C_{pl} \Delta T}{C_{sf} h_{fg} Pr^{ns}} \right]^3 \quad (13)$$

where  $\rho_l$ ,  $\rho_v$ ,  $g$ ,  $h_{fg}$ ,  $\mu_l$  and  $\sigma_{lv}$  are density of fluid, vapor density, gravitational acceleration, heat of vaporization, viscosity and surface tension, respectively.  $Pr$ ,  $\Delta T$ ,  $C_{pl}$ , are Prandtl number, excess temperature, and heat capacity of fluid.  $ns$  and  $C_{sf}$  are experimental constants that depend on the boiling surface and liquid. For example, water/aluminum plate ( $Ra = 3.61 \mu\text{m}$ ),  $C_{sf}$  and  $ns$  are 0.011 and 1.26, respectively [83]. From the above equation, it can be easily deduced that the increase in the viscosity and wettability of the nanofluid conducts more heat flux than the base fluid at the same superheat temperature. Additionally, these nanoparticles act as porous conductive layers on the heating surface, enhancing boiling heat transfer [79,81].

Kim et al. [84] studied the effect of aqueous nanofluids composed of alumina, zirconia and silica nanoparticles on nucleate boiling. The volume fraction of nanoparticles varied from 0.001 to 1.0% by volume. Pool boiling studies were performed on stainless steel grade 316. Significant improvements of up to 200% in critical heat flux (CHF) were observed using the various nanoparticles shown in in Figure 7a. The wettability of fluid with the SS316 wire was observed to increase with the addition of nanoparticles. As shown in Figure 7b,d, vapor bubbles were uniformly distributed on the heater surface and CHF increased. Sarafraz et al. [79] conducted experiments on pool boiling heat transfer around a stainless steel cylindrical surface in aqueous nanofluids varying the CuO particle fraction

from 0.1 to 0.4 wt.%. Sodium deodecyl sulphide solution of 0.1% was added for steric stabilization, and HCl + NaOH buffer solution was added for electrostatic stabilization to change the pH. They have reported a decrease in pool boiling heat transfer coefficient due to the deposition of nanoparticles on the heat transfer surface. Many researchers have observed the enhancement in critical heat flux during pool boiling heat transfer for all nanofluids [85]. This is because the surface tension decreases due to the increase in wettability and the surface roughness decreases due to the deposition of nanoparticles in the micro cavity around the heating section.

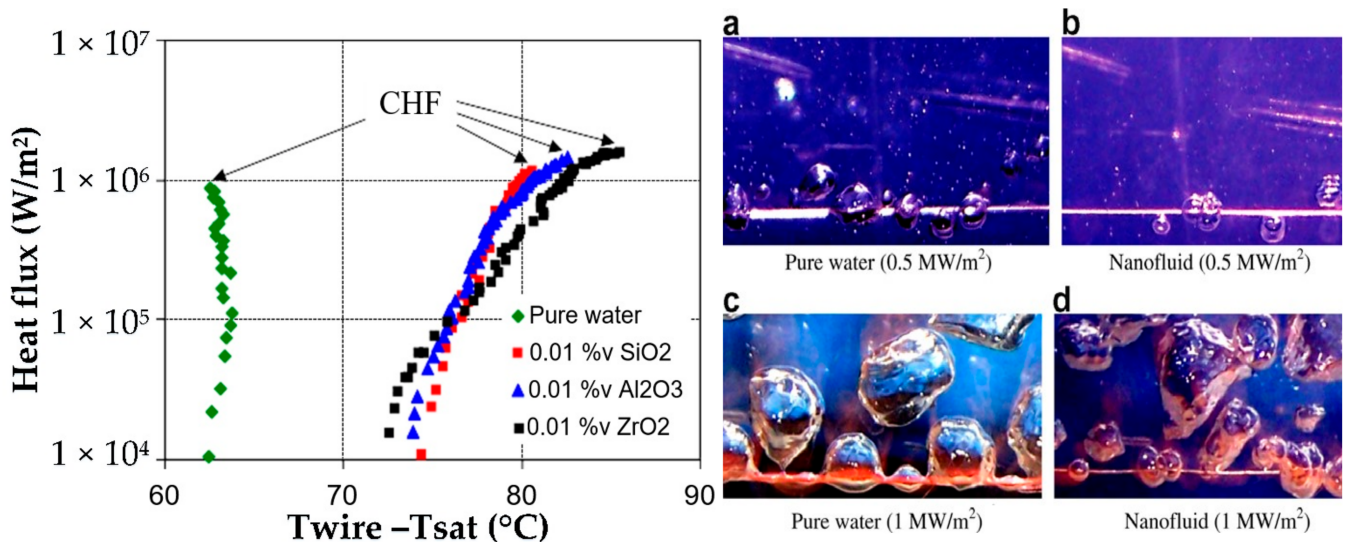


**Figure 7.** Boiling curves for stainless steel wire; pool boiling of pure water and 0.01 vol.% alumina nanofluid at the same heat flux on stainless steel wire [84]. (a–d) presents the pool boiling response of fluid bubbles at same heat flux around the stainless steel wire.

The interaction between two immiscible phases creates interfacial energy. Low interfacial energy induces attraction and high interfacial energy induces repulsion. The interaction of these interfacial forces can be described using Young's equation.

$$\cos \theta = \frac{\sigma_{SV} - \sigma_{SL}}{\sigma_{LV}} \quad (14)$$

where  $\theta$  denotes the contact angle,  $(\sigma_{SV} - \sigma_{SL})$  is adhesion tension, and  $\sigma_{LV}$  is the surface tension.

As the surface roughness increases, the nucleation site density increases, resulting in increased boiling heat transfer. Wen et al. [86] observed different CHF's for smooth and rough boiling surfaces on square copper and aluminum plates of size  $50 \times 50 \text{ mm}^2$  for the same surfactant solution.

This is because an increase in the nucleate site density and a decrease in the contact angle for rough surfaces enhances the activation of nucleation sites. Similar results are also supported by the pool boiling of metal oxide-based nanofluids [87,88]. Young's equation is not sufficient to evaluate the pool boiling characteristics of nanofluids. Therefore, Wenzel [89] investigated the effect of surface roughness on the equilibrium contact angle and modified the Young's equation as follows.

$$\cos \theta^* = \left( \frac{\sigma_{SV} - \sigma_{SL}}{\sigma_{LV}} \right) r \quad (15)$$

where  $r$  is the roughness ratio, i.e., the ratio between actual and projected surface area. Figure 8 presents the schematic illustration of nucleate boiling contact angle according to Wenzel.

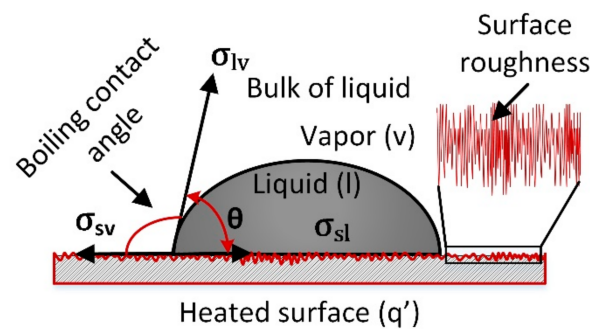


**Figure 8.** Nucleate boiling contact angle according to Wenzel.

### 3.5. Effect of Nanoparticle Geometry

The shape of nanoparticles has a significant impact on the thermal performance of the thermal systems containing nanofluids. Elena et al. [50] assessed the thermal conductivity and viscosity of EG/H<sub>2</sub>O-based suspensions (50:50) depending on the shape of polycrystalline Al<sub>2</sub>O<sub>3</sub> nanoparticles (platelets, bricks, cylinders and blades). The effective theoretical thermal conductivity of nanofluids was calculated by using Hamilton–Crosser model including the empirical shape factor  $n$  (given in Table 2). In Table 2,  $\psi$  is defined as the ratio of the spherical surface area to the surface area of real particles of the same volume. This theoretical prediction of thermal conductivity was in good agreement with the experimental results. The improvement of thermal conductivity showed the following order: platelets  $\approx$  blades < bricks < cylinders. The experimental viscosity improvement showed the following sequence: blades < bricks < cylinders < platelets.

Mehdi et al. [90] investigated the entropy generation of water–alumina nanofluids with various nanoparticle shapes (platelet, brick, cylinder, blade and oblate spheroid) at four Reynolds numbers ( $Re = 300, 800, 1300$  and  $1800$ , respectively). They analyzed the effect of nanofluids on total entropy generation for a micro heat sink made of silicon. The lowest and highest thermal entropy generation was observed for platelet-based and oblate spheroid-based nanofluids, respectively, at large Reynolds number. It was also observed that the large surface area of cylindrical nanoparticles raised the viscosity of nanofluids, increasing the frictional entropy of the system.

Sheikholeslami et al. [91] investigated the effect of CuO aqueous nanofluids on a uniform magnetic field in a porous semi-annulus system. The effect of nanoparticles of different shapes (platelets, bricks, cylinders and spheres) on Nusselt number was analyzed. They observed a higher rate of heat transfer in the platelet-shaped nanoparticles for the same volume fraction.

Abassi et al. [92] performed molecular dynamics simulations on the attraction of base fluids towards distinct nanoparticle shapes (planar, rod, sphere and block). Different shapes attracted the base fluid in different ways. They concluded that planar nanoparticles had the highest density of base fluid layer compared to spherical and rod-shaped particles due to their flat surfaces with no curvature.

Maheshwari et al. [93] performed a comprehensive study of the effect of particle shape (spherical, cubic and rod) on the thermal conductivity of TiO<sub>2</sub> aqueous nanofluids. The pumping power, viscosity and thermal conductivity of cubic-shaped nanoparticles are the highest among all types. The large surface area of the cubic-shaped nanoparticles contributed to the improvement of the thermal transport properties of the cubic-shaped TiO<sub>2</sub>-water-based nanofluids.

In most previous investigations, platelet-type nanoparticles lead to the best heat transfer performance. This may be due to its highest shape factor with increased contact area which increases the Brownian velocity inside the base fluid, leading to higher heat transfer rate [94].

### 3.6. Economic Analysis

The increased efficiency of nanofluids enables compact designs of heat transfer systems in a variety of industrial systems without affecting the desired output. Smaller systems can significantly reduce the manufacturing costs. For example, Al<sub>2</sub>O<sub>3</sub>-H<sub>2</sub>O-based flat plate solar collectors have reduced the solar collector area by 21.5% [95]. In addition to scientific and technical aspects, cost effectiveness should be analyzed both in terms of expenses and performance. The global prices of selected metal oxide-based nanoparticles are shown in Table 5. The cost increment must be persuasive, through a price/performance analysis, for economic justification to the industry. This can be calculated as the Efficiency Price Index (EPI), which is defined as [96]:

$$EPI = \frac{\eta}{price} \times 1000 \quad (16)$$

where  $\eta$  is the thermal efficiency of heat transfer system which is defined as [97]:

$$\eta = \frac{(Nu_{nf}/Nu_{bf})}{(f_{nf}/f_{bf})^{1/3}} \quad (17)$$

where  $f$  is the friction factor of a heat transfer system. The higher the EPI index, the higher the industrial applicability of nanofluids.

**Table 5.** Price of some oxide-based nanoparticles [96].

Nanoparticle	Price (\$/10 g)
TiO <sub>2</sub>	96.81
MgO	170.5
ZnO	79
CuO	68
Fe <sub>2</sub> O <sub>3</sub>	31.4
Al <sub>2</sub> O <sub>3</sub>	7.8
Fe <sub>3</sub> O <sub>4</sub>	16.8

Abazar et al. [98] performed an economic analysis of metal oxide water-based photo-voltaic thermal systems (PVTs). They formulated the nanofluids by selecting 0.2 wt.% ZnO, Al<sub>2</sub>O<sub>3</sub>, and TiO<sub>2</sub> nanoparticles. Out of these, PVT-ZnO has the largest annual energy cost saving of 33% compared to the conventional pure water-based system. The payback period for this PVT-ZnO system is approximately 4.3 years. Esfe et al. [97] conducted a multi-objective optimization of the cost and thermal performance of double-walled CNT/water nanofluids. Thermal performance factors of nanofluids were obtained at different Reynolds numbers and volume fractions in experiments performed at constant wall heat flux in the laminar flow regime inside a copper tube (length 1000 mm and diameter 7 mm). The thermal performance factor was evaluated from the ratio of the Nusselt number to the friction factor of the pumping power. From the multi-objective response surface method, they observed that it costs \$504 per liter to achieve a thermal performance factor of 1.197 in their system. Alirezaie et al. [99] evaluated the price/performance ratio of EG/MgO and EG/Fe nanofluids with varying particle sizes from 20 nm to 60 nm. The smaller the size of nanoparticles, the higher the cost. They concluded that MgO nanofluids are more cost-effective in terms of heat transfer efficiency than Fe-based nanofluids.

According to the report from International Energy Agency (IEA), in 2019, space heating accounted for a major share of thermal energy consumption in the industrial and residential sectors [100]. For example, a residential house consumes on average monthly electricity in the range of 500–10,000 kWh, depending on the climate. Let us assume a home with an average annual energy consumption of 5000 kWh. If the heating system requires 15 L of H<sub>2</sub>O/Al<sub>2</sub>O<sub>3</sub>-based nanofluid with 0.02 vol.%, the total cost of the nanofluid would be 720 USD. If the average electricity price in the US is 12 cents per kWh and the total annual

cost of electricity is 600 USD, the average efficiency increase of Al<sub>2</sub>O<sub>3</sub> aqueous nanofluids in heat exchanger systems is 25% [100]. The average savings from using nanofluids is \$150 per year. So, after 5 years, you can achieve a capital return on your \$720 investment.

### 3.7. Heat Transfer Merit

After careful evaluation of the thermophysical properties of nanofluids, the feasibility of using nanofluids instead of base fluids for heat transfer applications should be evaluated. In addition, to optimize the overall performance of nanofluids for industrial applications, the heat transfer efficiency in the laminar and turbulent regimes should be analyzed. The heat transfer potential of nanofluids in laminar flow is described by Parashar et al. [101].

$$C_o = \frac{C_\mu}{C_k} = \frac{(\mu_{nf} - \mu_{bf}) / \mu_{bf}}{(k_{nf} - k_{bf}) / k_{bf}} \quad (18)$$

If  $C_\mu/C_k < 4$ , the nanofluid is effective in the laminar flow regime, and if  $C_\mu/C_k > 4$ , the nanosuspension is ineffective in the laminar flow regime.

The heat transfer efficiency of nanofluids under turbulent flow can be determined from the Mouromtseff number [102] given below.

$$M_o = \frac{\rho^{0.8} k^{0.67} C_p^{0.33}}{\mu^{0.4}} \quad (19)$$

If the Mouromtseff number ratio ( $M_{onf}/M_{obf}$ ) is greater than 1, nanofluids are considered better heat transfer media compared to basic fluids. The higher the Mo number, the higher the heat transfer performance of the nanofluid.

## 4. Future Scope and Challenges for Nanofluid Applications in Various Industrial Sectors

A high-efficiency heat transfer device applied to a thermal system is a heat pipe. It uses a phase change in the working fluid to transfer heat. Yang et al. [103] evaluated the heat transfer performance of a horizontal microgroove heat pipe using various nanofluids containing 0.5 to 2.0 wt.% CuO. At an optimal concentration of 1.0 wt.% CuO, they observed an average of 46% and 30% improvement in heat transfer coefficient and CHF, respectively. Khandaker et al. [104] investigated the two-phase thermal performance of thermosiphons using aqueous Al<sub>2</sub>O<sub>3</sub> and CuO nanofluids. They observed an increase in the wettability of nanofluids on copper substrates compared to the base fluid. Al<sub>2</sub>O<sub>3</sub>-based nanofluids showed better wettability. However, entrapment of these nanoparticles in the surface roughness reduced active bubble nucleation sites and weakened thermal performance in closed-loop thermosiphons. The electronics industry has grown significantly over the past few decades, and cooling has emerged as a major issue affecting the overall performance of a system. The high heat flux generated by the processor chip must be cooled rapidly to achieve the expected efficiency and reliability. Mini- and micro-channel-based cooling systems are the most efficient ones in modern electronics. The most-used materials for electronic cooling are Al<sub>2</sub>O<sub>3</sub> and TiO<sub>2</sub>-based nanofluids [105]. Nazari et al. [106] investigated Al<sub>2</sub>O<sub>3</sub>-ethyleneglycol/water-based nanofluids for CPU cooling. A decrease in the final process temperature and an increase in the convective heat transfer coefficient were also observed. At 0.5 vol.% Al<sub>2</sub>O<sub>3</sub> particles, a 6% increase in heat transfer coefficient was observed compared to the base fluid. The thermal and hydraulic performance of micro-fin heat sinks were numerically investigated using static and dynamic single-phase models by Guo et al. [107]. They used ZnO aqueous nanofluids. As the volume fraction increased from 1.5% to 3.0%, the heat transfer coefficient increased from 4300 to 11,470 W/m<sup>2</sup>K. Khani et al. [108] experimentally investigated the heat transfer performance of Al<sub>2</sub>O<sub>3</sub> (35 nm) and TiO<sub>2</sub> (50 nm) nanofluids through spiral coiled tubes over a wide range of Reynolds numbers (50–4500). Nanoparticles of 0.25–1.0% volume fraction were dispersed and suspended in

water. Triton X-100 and Cetyltrimethylammonium Bromide were used as stabilizers for  $\text{Al}_2\text{O}_3$  and  $\text{TiO}_2$  nanofluids. Due to the higher thermal conductivity of  $\text{Al}_2\text{O}_3$  particles, the heat transfer performance improvement of  $\text{Al}_2\text{O}_3$  dispersions were higher than that of  $\text{TiO}_2$  nanofluids. The  $\text{Al}_2\text{O}_3$  nanofluid of 1.0 vol.% showed the maximum performance at  $\text{Re} = 1865$ . Moreover, the pressure drop is greatly increased when the nanoparticle concentration is above 1.0%.

Various nanoparticle-enhanced coolants based on metal oxides are used in a variety of machining processes, such as drilling, milling, grinding, and turning. Compared with conventional flood cooling and dry machining, nanofluid machining provides better surface finish and cooling efficiency. Vasu et al. [109] analyzed the effect of  $\text{Al}_2\text{O}_3$ -TRIM E709 emulsifier nanofluid as a cutting lubricant in the grinding of EN-31 steel. The high specific energy requirements for grinding lead to the development of high temperatures in the grinding zone. Compared to plain emulsifiers, nano lubricants lowered the wheel working parts temperature by 20% to 30%. Najiha et al. [110] investigated the flank wear rates of Al-6061 alloys using aqueous  $\text{TiO}_2$  nano-minimum quantity lubrication (MQL). By adding 1.5% volume fraction nanoparticles, it was compared with conventional oil-based MQL. Compared to conventional oil-based lubricants, less edge chipping of cutting tools was observed. This was because the higher cooling rate of the nanofluid preserved the edge integrity of the cutting tool. Recently, Sujith et al. [111] evaluated the effectiveness of pure coconut oil  $\text{Al}_2\text{O}_3$  nanofluids on the turning of Al-7079 TiC in-situ metal matrix composites. The nanoparticle concentration was varied from 0.1–0.6 vol.%. The presence of highly conductive alumina particles significantly reduced the cutting zone temperature. However, when the particle concentration was above 0.4%, the heat transfer efficiency of the cutting fluid decreased due to the reduced fluidity of the lubricant between the tool chip interfaces.

So far, few investigations have been made on the effect of particle shape on the heat transfer properties of nanofluids. Future studies should elucidate the particle shape effects and their dynamics in various base fluids followed by heat transfer analysis. The thermo-physical characterization of the particle shape effect on the hydrothermal performance of a heat transfer system is mostly a theoretical study. Therefore, there is a need for experimental studies on distinct particle shapes for different nanoparticles for various nanofluids. In the past few years, few studies have focused on the development of hybrid nanofluids involving the co-dispersion of metal-based and metal oxide-based nanofluids to achieve long-term stability and low viscosity along with higher thermal conductivity [112]. When using hybrid nanofluids, the physical and chemical compatibility between different types of nanoparticles is an important factor to consider [113] and therefore needs to be further studied both theoretically and experimentally.

## 5. Conclusions

This study presents a comprehensive review on the preparation and application of metal oxide-based nanofluids, especially on heat transfer application. Due to their chemical inertness and ability to enhance the thermophysical properties of heat transfer fluids, metal oxide-based nanofluids have attracted considerable attention in a variety of heat transfer applications. For the wide application of nanofluids by commercialization, several key challenges such as stability and production cost must be analyzed.

For example, the main heat transfer mechanisms in heat pipes are convective evaporation and convective condensation during boiling. A variety of industrial heat pipes include capillary pump loop (CPL) heat pipes, flat shaped axial heat pipes, and ordinary cylindrical heat pipes [114–116]. The addition of nanoparticles to the base fluid improved the heat transfer performance to a greater extent. The increase in wettability due to the addition of nanoparticles also increased the capillary force of the CPL pipe, but it increased the viscosity and density to increase the flow resistance as well. Therefore, it is necessary to determine the optimal concentration of nanoparticles to balance drag and capillary forces. In the case of the pool boiling process, the boiling characteristics are governed by the nanoparticles, the stabilizers and the affinity of base fluid and heater. A thin layer of porous sediment can

form on the heater surface, reducing the number of active nucleation sites [79]. In addition, sedimentation of nanoparticles can reduce the half cone angle of the roughness cavity and reduce the number of active nucleation sites. The reduction in the number of active nucleation sites weakens heat transfer. Various nanofluid formulations exist to improve heat transfer and lubrication performance in machining processes [117,118]. The efficiency and reliability of machine tools are greatly improved by nanofluids. The direction of future nanofluid studies should mainly be to find the optimal nanoparticle group, nanoparticle size, stabilizer and various operating parameters such as temperature, concentration and ambient temperature. These will enable practical applications of nanofluids for improved heat transfer in a variety of engineering applications.

**Author Contributions:** Conceptualization, S.V.S. and J.L.; writing—original draft preparation, S.V.S.; writing—review and editing, H.K.; visualization, S.V.S.; supervision, H.K. and J.L.; funding acquisition, J.L. All authors have read and agreed to the published version of the manuscript.

**Funding:** This research was funded by the Competency Development Program for Industry Specialists of the Korea Institute for Advancement of Technology, grant number P0002019.

**Institutional Review Board Statement:** Not applicable.

**Informed Consent Statement:** Not applicable.

**Data Availability Statement:** Data sharing is not applicable.

**Conflicts of Interest:** The authors declare no conflict of interest.

## Nomenclature

$d$	diameter
$K$	thermal conductivity
$T$	temperature
$C_p$	specific heat
$K_b$	Boltzmann constant
$Re$	Reynolds number
$Pr$	Prandtl number
$m$	mass
$f$	friction factor

### Greek symbols

$\rho$	density
$\mu$	viscosity
$\Phi$	solid volume fraction
$\alpha$	thermal diffusivity
$\eta$	efficiency

### Subscripts/superscripts

$bf$	base fluid
$nf$	nanofluid
$ns$	nano structure
$fr$	freezing point
$p$	particle

## References

1. Lund, H.; Werner, S.; Wiltshire, R.; Svendsen, S.; Thorsen, J.E.; Hvelplund, F.; Mathiesen, B.V. 4th Generation District Heating (4GDH). Integrating smart thermal grids into future sustainable energy systems. *Energy* **2014**, *68*, 1–11. [[CrossRef](#)]
2. Godson, L.; Raja, B.; Lal, D.M.; Wongwises, S. Enhancement of heat transfer using nanofluids—An overview. *Renew. Sustain. Energy Rev.* **2010**, *14*, 629–641. [[CrossRef](#)]
3. Bég, O.A.; Espinoza, D.E.S.; Kadir, A.; Shamshuddin, M.; Sohail, A. Experimental study of improved rheology and lubricity of drilling fluids enhanced with nano-particles. *Appl. Nanosci.* **2018**, *8*, 1069–1090. [[CrossRef](#)]
4. Sriharan, G.; Harikrishnan, S.; Ali, H.M. Experimental investigation on the effectiveness of MHTHS using different metal oxide-based nanofluids. *J. Therm. Anal.* **2021**, *143*, 1251–1260. [[CrossRef](#)]

5. Jamshed, W.; Şirin, C.; Selimefendigil, F.; Shamshuddin, M.D.; Altowairqi, Y.; Eid, M.R. Thermal Characterization of Coolant Maxwell Type Nanofluid Flowing in Parabolic Trough Solar Collector (PTSC) Used Inside Solar Powered Ship Application. *Coatings* **2021**, *11*, 1552. [CrossRef]
6. Chandrasekar, M.; Suresh, S.; Bose, A.C. Experimental studies on heat transfer and friction factor characteristics of Al<sub>2</sub>O<sub>3</sub>/water nanofluid in a circular pipe under laminar flow with wire coil inserts. *Exp. Therm. Fluid Sci.* **2010**, *34*, 122–130. [CrossRef]
7. Murshed, S.M.S.; Leong, K.C.; Yang, C. Enhanced thermal conductivity of TiO<sub>2</sub>—Water based nanofluids. *Int. J. Therm. Sci.* **2005**, *44*, 367–373. [CrossRef]
8. Koshy, C.P.; Rajendrakumar, P.K.; Thottackkad, M.V. Evaluation of the tribological and thermo-physical properties of coconut oil added with MoS<sub>2</sub> nanoparticles at elevated temperatures. *Wear* **2015**, *330*, 288–308. [CrossRef]
9. Sujith, S.; Solanki, A.K.; Mulik, R.S. Experimental evaluation on rheological behavior of Al<sub>2</sub>O<sub>3</sub>-pure coconut oil nanofluids. *J. Mol. Liq.* **2019**, *286*, 110905. [CrossRef]
10. Esfe, M.H.; Arani, A.A.A.; Esfandeh, S. Experimental study on rheological behavior of monograde heavy-duty engine oil containing CNTs and oxide nanoparticles with focus on viscosity analysis. *J. Mol. Liq.* **2018**, *272*, 319–329. [CrossRef]
11. Nguyen, C.; Desgranges, F.; Roy, G.; Galanis, N.; Maré, T.; Boucher, S.; Mintsa, H.A. Temperature and particle-size dependent viscosity data for water-based nanofluids—Hysteresis phenomenon. *Int. J. Heat Fluid Flow* **2007**, *28*, 1492–1506. [CrossRef]
12. Nadooshan, A.A.; Esfe, M.H.; Afrand, M. Evaluation of rheological behavior of 10W40 lubricant containing hybrid nano-material by measuring dynamic viscosity. *Phys. E Low Dimens. Syst. Nanostruct.* **2017**, *92*, 47–54. [CrossRef]
13. Maxwell, J.C. *A Treatise on Electricity and Magnetism*; Cambridge University Press: Cambridge, UK, 1873. [CrossRef]
14. Choi, J.E.S. Enhancing Thermal Conductivity of Fluids with Nanoparticles. 1995. Available online: <https://www.osti.gov/biblio/196525-enhancing-thermal-conductivity-fluids-nanoparticles> (accessed on 10 December 2021).
15. Kim, S.H.; Choi, S.R.; Kim, D. Thermal conductivity of metal-oxide nanofluids: Particle size dependence and effect of laser irradiation. *J. Heat Transf.* **2007**, *129*, 298–307. [CrossRef]
16. Azmi, W.; Sharma, K.V.; Sarma, P.; Mamat, R.; Anuar, S.; Rao, V.D. Experimental determination of turbulent forced convection heat transfer and friction factor with SiO<sub>2</sub> nanofluid. *Exp. Therm. Fluid Sci.* **2013**, *51*, 103–111. [CrossRef]
17. Wei, B.; Zou, C.; Li, X. Experimental investigation on stability and thermal conductivity of diathermic oil based TiO<sub>2</sub> nanofluids. *Int. J. Heat Mass Transf.* **2017**, *104*, 537–543. [CrossRef]
18. Agarwal, R.; Verma, K.; Agrawal, N.K.; Duchaniya, R.K.; Singh, R. Synthesis, characterization, thermal conductivity and sensitivity of CuO nanofluids. *Appl. Therm. Eng.* **2016**, *102*, 1024–1036. [CrossRef]
19. Wang, X.-J.; Zhu, D.-S.; Yang, S. Investigation of pH and SDBS on enhancement of thermal conductivity in nanofluids. *Chem. Phys. Lett.* **2009**, *470*, 107–111. [CrossRef]
20. Colangelo, G.; Favale, E.; Miglietta, P.; Milanese, M.; De Risi, A. Thermal conductivity, viscosity and stability of Al<sub>2</sub>O<sub>3</sub>-diathermic oil nanofluids for solar energy systems. *Energy* **2016**, *95*, 124–136. [CrossRef]
21. Yu, F.; Chen, Y.; Liang, X.; Xu, J.; Lee, C.; Liang, Q.; Tao, P.; Deng, T. Dispersion stability of thermal nanofluids. *Prog. Nat. Sci. Mater. Int.* **2017**, *27*, 531–542. [CrossRef]
22. Zheng, T.; Bott, S.; Huo, Q. Techniques for accurate sizing of gold nanoparticles using dynamic light scattering with particular application to chemical and biological sensing based on aggregate formation. *ACS Appl. Mater. Interfaces* **2016**, *8*, 21585–21594. [CrossRef] [PubMed]
23. Mehrali, M.; Sadeghinezhad, E.; Latibari, S.T.; Kazi, S.N.; Mehrali, M.; Zubir, M.N.B.M.; Metselaar, H.S.C. Investigation of thermal conductivity and rheological properties of nanofluids containing graphene nanoplatelets. *Nanoscale Res. Lett.* **2014**, *9*, 15. [CrossRef]
24. Malescio, G. Intermolecular potentials—Past, present, future. *Nat. Mater.* **2003**, *2*, 501–503. [CrossRef] [PubMed]
25. Lunardi, C.N.; Gomes, A.J.; Rocha, F.S.; De Tommaso, J.; Patience, G.S. Experimental methods in chemical engineering: Zeta potential. *Can. J. Chem. Eng.* **2021**, *99*, 627–639. [CrossRef]
26. Ohshima, H. Henry's function for electrophoresis of a cylindrical colloidal particle. *J. Colloid Interface Sci.* **1996**, *180*, 299–301. [CrossRef]
27. Qi, C.; Luo, T.; Liu, M.; Fan, F.; Yan, Y. Experimental study on the flow and heat transfer characteristics of nanofluids in double-tube heat exchangers based on thermal efficiency assessment. *Energy Convers. Manag.* **2019**, *197*, 111877. [CrossRef]
28. Xuan, Y.; Li, Q. Investigation on convective heat transfer and flow features of nanofluids. *J. Heat Transf.* **2003**, *125*, 151–155. [CrossRef]
29. Pak, B.C.; Cho, Y.I. Hydrodynamic and heat transfer study of dispersed fluids with submicron metallic oxide particles. *Exp. Heat Transf.* **1998**, *11*, 151–170. [CrossRef]
30. Vajjha, R.S.; Das, D.K. Specific heat measurement of three nanofluids and development of new correlations. *J. Heat Transf.* **2009**, *131*, 071601. [CrossRef]
31. Zhou, L.-P.; Wang, B.-X.; Peng, X.-F.; Du, X.-Z.; Yang, Y.-P. On the specific heat capacity of CuO nanofluid. *Adv. Mech. Eng.* **2010**, *2010*, 172085. [CrossRef]
32. Sekhar, Y.R.; Sharma, K.V. Study of viscosity and specific heat capacity characteristics of water-based Al<sub>2</sub>O<sub>3</sub> nanofluids at low particle concentrations. *J. Exp. Nanosci.* **2013**, *10*, 86–102. [CrossRef]
33. Shin, D.; Banerjee, D. Specific heat of nanofluids synthesized by dispersing alumina nanoparticles in alkali salt eutectic. *Int. J. Heat Mass Transf.* **2014**, *74*, 210–214. [CrossRef]

34. Cabaleiro, D.; Gracia-Fernández, C.; Legido, J.; Lugo, L. Specific heat of metal oxide nanofluids at high concentrations for heat transfer. *Int. J. Heat Mass Transf.* **2015**, *88*, 872–879. [[CrossRef](#)]
35. Barbés, B.; Páramo, R.; Blanco, E.; Casanova, C. Thermal conductivity and specific heat capacity measurements of CuO nanofluids. *J. Therm. Anal.* **2014**, *115*, 1883–1891. [[CrossRef](#)]
36. Murshed, S.S. Determination of effective specific heat of nanofluids. *J. Exp. Nanosci.* **2011**, *6*, 539–546. [[CrossRef](#)]
37. Shin, D.; Tiznobaik, H.; Banerjee, D. Specific heat mechanism of molten salt nanofluids. *Appl. Phys. Lett.* **2014**, *104*, 121914. [[CrossRef](#)]
38. Tiznobaik, H.; Banerjee, D.; Shin, D. Effect of formation of “long range” secondary dendritic nanostructures in molten salt nanofluids on the values of specific heat capacity. *Int. J. Heat Mass Transf.* **2015**, *91*, 342–346. [[CrossRef](#)]
39. Hassan, M.A.; Banerjee, D. A soft computing approach for estimating the specific heat capacity of molten salt-based nanofluids. *J. Mol. Liq.* **2019**, *281*, 365–375. [[CrossRef](#)]
40. Ercole, D.; Manca, O.; Vafai, K. An investigation of thermal characteristics of eutectic molten salt-based nanofluids. *Int. Commun. Heat Mass Transf.* **2017**, *87*, 98–104. [[CrossRef](#)]
41. Sang, L.; Liu, T. The enhanced specific heat capacity of ternary carbonates nanofluids with different nanoparticles. *Sol. Energy Mater. Sol. Cells* **2017**, *169*, 297–303. [[CrossRef](#)]
42. Qiao, G.; Lasfargues, M.; Alexiadis, A.; Ding, Y. Simulation and experimental study of the specific heat capacity of molten salt based nanofluids. *Appl. Therm. Eng.* **2017**, *111*, 1517–1522. [[CrossRef](#)]
43. Hamilton, R.L.; Crosser, O.K. Thermal Conductivity of Heterogeneous Two-Component Systems. *Ind. Eng. Chem. Fundam.* **1962**, *1*, 187–191. [[CrossRef](#)]
44. Bruggeman, D.A.G. Berechnung verschiedener physikalischer konstanten von heterogenen substanzen. I. dielektrizitätskonstanten und leitfähigkeiten der mischkörper aus isotropen Substanzen. *Ann. Phys.* **1935**, *416*, 636–664. [[CrossRef](#)]
45. Akita, O.; Yamada, E. Effective thermal conductivity of dispersed materials. *Heat Mass Transf.* **1980**, *13*, 27–37.
46. Sujith, S.V.; Solanki, A.K.; Mulik, R.S. Experimental evaluation in thermal conductivity enhancement and heat transfer optimization of eco-friendly Al<sub>2</sub>O<sub>3</sub>–pure coconut oil based nano fluids. *J. Therm. Sci. Eng. Appl.* **2021**, *13*, 1–13. [[CrossRef](#)]
47. Yu, W.; Choi, S.U.S. The role of interfacial layers in the enhanced thermal conductivity of nanofluids: A renovated Maxwell model. *J. Nanopart. Res.* **2003**, *5*, 167–171. [[CrossRef](#)]
48. Yoo, D.-H.; Hong, K.; Yang, H.-S. Study of thermal conductivity of nanofluids for the application of heat transfer fluids. *Thermochim. Acta* **2007**, *455*, 66–69. [[CrossRef](#)]
49. Esfe, M.H.; Amiri, M.K.; Alirezaie, A. Thermal conductivity of a hybrid nanofluid. *J. Therm. Anal. Calorim.* **2018**, *134*, 1113–1122. [[CrossRef](#)]
50. Timofeeva, E.V.; Routbort, J.L.; Singh, D. Particle shape effects on thermophysical properties of alumina nanofluids. *J. Appl. Phys.* **2009**, *106*, 014304. [[CrossRef](#)]
51. Koo, J.; Kleinstreuer, C. A new thermal conductivity model for nanofluids. *J. Nanopart. Res.* **2004**, *6*, 577–588. [[CrossRef](#)]
52. Khdher, A.M.; Sidik, N.A.C.; Hamzah, W.A.W.; Mamat, R. An experimental determination of thermal conductivity and electrical conductivity of bio glycol based Al<sub>2</sub>O<sub>3</sub> nanofluids and development of new correlation. *Int. Commun. Heat Mass Transf.* **2016**, *73*, 75–83. [[CrossRef](#)]
53. Lu, S.; Lin, H. Effective conductivity of composites containing aligned spheroidal inclusions of finite conductivity. *J. Appl. Phys.* **1996**, *79*, 6761–6769. [[CrossRef](#)]
54. Krieger, I.M.; Dougherty, T.J. A mechanism for non-newtonian flow in suspensions of rigid spheres. *Trans. Soc. Rheol.* **1959**, *3*, 137–152. [[CrossRef](#)]
55. Chhabra, R.P. Non-newtonian fluids: An introduction. In *Rheology Complex Fluids*; Springer: New York, NY, USA, 2010; pp. 3–34. [[CrossRef](#)]
56. Esfe, M.H.; Rostamian, H. Non-Newtonian power-law behavior of TiO<sub>2</sub> /SAE 50 nano-lubricant: An experimental report and new correlation. *J. Mol. Liq.* **2017**, *232*, 219–225. [[CrossRef](#)]
57. Sharma, A.K.; Tiwari, A.K.; Dixit, A.R. Rheological behaviour of nanofluids: A review. *Renew. Sustain. Energy Rev.* **2015**, *53*, 779–791. [[CrossRef](#)]
58. Hu, X.; Yin, D.; Chen, X.; Xiang, G. Experimental investigation and mechanism analysis: Effect of nanoparticle size on viscosity of nanofluids. *J. Mol. Liq.* **2020**, *314*, 113604. [[CrossRef](#)]
59. Mostafizur, R.; Aziz, A.A.; Saidur, R.; Bhuiyan, M.; Mahbubul, I. Effect of temperature and volume fraction on rheology of methanol based nanofluids. *Int. J. Heat Mass Transf.* **2014**, *77*, 765–769. [[CrossRef](#)]
60. Chiam, H.; Azmi, W.; Usri, N.; Mamat, R.; Adam, N. Thermal conductivity and viscosity of Al<sub>2</sub>O<sub>3</sub> nanofluids for different based ratio of water and ethylene glycol mixture. *Exp. Therm. Fluid Sci.* **2017**, *81*, 420–429. [[CrossRef](#)]
61. Fedele, L.; Colla, L.; Bobbo, S. Viscosity and thermal conductivity measurements of water-based nanofluids containing titanium oxide nanoparticles. *Int. J. Refrig.* **2012**, *35*, 1359–1366. [[CrossRef](#)]
62. Moldoveanu, G.M.; Ibanescu, C.; Danu, M.; Minea, A.A. Viscosity estimation of Al<sub>2</sub>O<sub>3</sub>, SiO<sub>2</sub> nanofluids and their hybrid: An experimental study. *J. Mol. Liq.* **2018**, *253*, 188–196. [[CrossRef](#)]
63. Ilyas, S.U.; Narahari, M.; Theng, J.T.Y.; Pendyala, R. Experimental evaluation of dispersion behavior, rheology and thermal analysis of functionalized zinc oxide-paraffin oil nanofluids. *J. Mol. Liq.* **2019**, *294*, 111613. [[CrossRef](#)]

64. Yan, S.-R.; Kalbasi, R.; Nguyen, Q.; Karimipour, A. Rheological behavior of hybrid MWCNTs-TiO<sub>2</sub>/EG nanofluid: A comprehensive modeling and experimental study. *J. Mol. Liq.* **2020**, *308*, 113058. [[CrossRef](#)]
65. Kole, M.; Dey, T. Effect of aggregation on the viscosity of copper oxide—gear oil nanofluids. *Int. J. Therm. Sci.* **2011**, *50*, 1741–1747. [[CrossRef](#)]
66. Çolak, A.B. A novel comparative analysis between the experimental and numeric methods on viscosity of zirconium oxide nanofluid: Developing optimal artificial neural network and new mathematical model. *Powder Technol.* **2021**, *381*, 338–351. [[CrossRef](#)]
67. Sonawane, S.S.; Juwar, V. Optimization of conditions for an enhancement of thermal conductivity and minimization of viscosity of ethylene glycol based Fe<sub>3</sub>O<sub>4</sub> nanofluid. *Appl. Therm. Eng.* **2016**, *109*, 121–129. [[CrossRef](#)]
68. Einstein, A. Eine neue bestimmung der moleküldimensionen. *Ann. Phys.* **1906**, *324*, 289–306. [[CrossRef](#)]
69. Brinkman, H.C. The viscosity of concentrated suspensions and solutions. *J. Chem. Phys.* **1952**, *20*, 571. [[CrossRef](#)]
70. Lundgren, T.S. Slow flow through stationary random beds and suspensions of spheres. *J. Fluid Mech.* **1972**, *51*, 273–299. [[CrossRef](#)]
71. Batchelor, G.K. The effect of Brownian motion on the bulk stress in a suspension of spherical particles. *J. Fluid Mech.* **1977**, *83*, 97–117. [[CrossRef](#)]
72. Wang, X.; Xu, X.; Choi, S.U.S. Thermal conductivity of nanoparticle—Fluid mixture. *J. Thermophys. Heat Transf.* **1999**, *13*, 474–480. [[CrossRef](#)]
73. Corcione, M. Empirical correlating equations for predicting the effective thermal conductivity and dynamic viscosity of nanofluids. *Energy Convers. Manag.* **2011**, *52*, 789–793. [[CrossRef](#)]
74. Namburu, P.K.; Kulkarni, D.P.; Misra, D.; Das, D.K. Viscosity of copper oxide nanoparticles dispersed in ethylene glycol and water mixture. *Exp. Therm. Fluid Sci.* **2007**, *32*, 397–402. [[CrossRef](#)]
75. Masoumi, N.; Sohrabi, N.; Behzadmehr, A. A new model for calculating the effective viscosity of nanofluids. *J. Phys. D Appl. Phys.* **2009**, *42*, 055501. [[CrossRef](#)]
76. Thomas, C.U.; Muthukumar, M. Three-body hydrodynamic effects on viscosity of suspensions of spheres. *J. Chem. Phys.* **1991**, *94*, 5180–5189. [[CrossRef](#)]
77. Graham, A.L. On the viscosity of suspensions of solid spheres. *Appl. Sci. Res.* **1981**, *37*, 275–286. [[CrossRef](#)]
78. Kim, S.J.; Bang, I.C.; Buongiorno, J.; Hu, L.W. Effects of nanoparticle deposition on surface wettability influencing boiling heat transfer in nanofluids. *Appl. Phys. Lett.* **2006**, *89*, 153107. [[CrossRef](#)]
79. Sarafraz, M.; Hormozi, F. Pool boiling heat transfer to dilute copper oxide aqueous nanofluids. *Int. J. Therm. Sci.* **2015**, *90*, 224–237. [[CrossRef](#)]
80. Zhang, F.; Jacobi, A.M. Aluminum surface wettability changes by pool boiling of nanofluids. *Colloids Surfaces A Physicochem. Eng. Asp.* **2016**, *506*, 438–444. [[CrossRef](#)]
81. Li, S.-Y.; Ji, W.-T.; Zhao, C.-Y.; Zhang, H.; Tao, W.-Q. Effects of magnetic field on the pool boiling heat transfer of water-based  $\alpha$ -Fe<sub>2</sub>O<sub>3</sub> and  $\gamma$ -Fe<sub>2</sub>O<sub>3</sub> nanofluids. *Int. J. Heat Mass Transf.* **2019**, *128*, 762–772. [[CrossRef](#)]
82. Rohsenow, V.M. *A Method of Correlating Heat Transfer Data for Surface Boiling of Liquids*; MIT Div. Ind. Cooperation: Cambridge, MA, USA, 1951; p. 31. Available online: <https://dspace.mit.edu/handle/1721.1/61431> (accessed on 10 December 2021).
83. Pioro, I. Experimental evaluation of constants for the Rohsenow pool boiling correlation. *Int. J. Heat Mass Transf.* **1998**, *42*, 2003–2013. [[CrossRef](#)]
84. Kim, S.; Bang, I.; Buongiorno, J.; Hu, L. Surface wettability change during pool boiling of nanofluids and its effect on critical heat flux. *Int. J. Heat Mass Transf.* **2007**, *50*, 4105–4116. [[CrossRef](#)]
85. Ciloglu, D.; Bolukbasi, A. A comprehensive review on pool boiling of nanofluids. *Appl. Therm. Eng.* **2015**, *84*, 45–63. [[CrossRef](#)]
86. Wen, D.; Wang, B. Effects of surface wettability on nucleate pool boiling heat transfer for surfactant solutions. *Int. J. Heat Mass Transf.* **2002**, *45*, 1739–1747. [[CrossRef](#)]
87. Wang, D.; Cheng, P. Effects of nanoparticles' wettability on vapor bubble coalescence in saturated pool boiling of nanofluids: A lattice Boltzmann simulation. *Int. J. Heat Mass Transf.* **2020**, *154*, 119669. [[CrossRef](#)]
88. Ji, W.-T.; Zhao, P.-F.; Zhao, C.-Y.; Ding, J.; Tao, W.-Q. Pool boiling heat transfer of water and nanofluid outside the surface with higher roughness and different wettability. *Nanoscale Microscale Thermophys. Eng.* **2018**, *22*, 296–323. [[CrossRef](#)]
89. Wenzel, R.N. Resistance of solid surfaces to wetting by water. *Ind. Eng. Chem.* **1936**, *28*, 988–994. [[CrossRef](#)]
90. Bahiraei, M.; Monavari, A.; Naseri, M.; Moayedi, H. Irreversibility characteristics of a modified microchannel heat sink operated with nanofluid considering different shapes of nanoparticles. *Int. J. Heat Mass Transf.* **2020**, *151*, 119359. [[CrossRef](#)]
91. Sheikholeslami, M.; Bhatti, M.M. Forced convection of nanofluid in presence of constant magnetic field considering shape effects of nanoparticles. *Int. J. Heat Mass Transf.* **2017**, *111*, 1039–1049. [[CrossRef](#)]
92. Abbasi, M.; Heyhat, M.; Rajabpour, A. Study of the effects of particle shape and base fluid type on density of nanofluids using ternary mixture formula: A molecular dynamics simulation. *J. Mol. Liq.* **2020**, *305*, 112831. [[CrossRef](#)]
93. Maheshwary, P.; Handa, C.; Nemade, K. A comprehensive study of effect of concentration, particle size and particle shape on thermal conductivity of titania/water based nanofluid. *Appl. Therm. Eng.* **2017**, *119*, 79–88. [[CrossRef](#)]
94. Zahmatkesh, I.; Sheremet, M.; Yang, L.; Heris, S.Z.; Sharifpur, M.; Meyer, J.P.; Ghalambaz, M.; Wongwises, S.; Jing, D.; Mahian, O. Effect of nanoparticle shape on the performance of thermal systems utilizing nanofluids: A critical review. *J. Mol. Liq.* **2021**, *321*, 114430. [[CrossRef](#)]

95. Faizal, M.; Saidur, R.; Mekhilef, S.; Alim, M. Energy, economic and environmental analysis of metal oxides nanofluid for flat-plate solar collector. *Energy Convers. Manag.* **2013**, *76*, 162–168. [[CrossRef](#)]
96. Alirezaie, A.; Hajmohammad, M.H.; Alipour, A.; Salari, M. Do nanofluids affect the future of heat transfer? “A benchmark study on the efficiency of nanofluids”. *Energy* **2018**, *157*, 979–989. [[CrossRef](#)]
97. Esfe, M.H.; Hajmohammad, H.; Moradi, R.; Arani, A.A.A. Multi-objective optimization of cost and thermal performance of double walled carbon nanotubes/water nanofluids by NSGA-II using response surface method. *Appl. Therm. Eng.* **2017**, *112*, 1648–1657. [[CrossRef](#)]
98. Abadeh, A.; Rejeb, O.; Sardarabadi, M.; Menezo, C.; Passandideh-Fard, M.; Jemni, A. Economic and environmental analysis of using metal-oxides/water nanofluid in photovoltaic thermal systems (PVTs). *Energy* **2018**, *159*, 1234–1243. [[CrossRef](#)]
99. Alirezaie, A.; Hajmohammad, M.H.; Ahangar, M.R.H.; Esfe, M.H. Price-performance evaluation of thermal conductivity enhancement of nanofluids with different particle sizes. *Appl. Therm. Eng.* **2018**, *128*, 373–380. [[CrossRef](#)]
100. Rios, M.S.B.-D.L.; Rivera-Solorio, C.I.; Nigam, K. An overview of sustainability of heat exchangers and solar thermal applications with nanofluids: A review. *Renew. Sustain. Energy Rev.* **2021**, *142*, 110855. [[CrossRef](#)]
101. Prasher, R.; Song, D.; Wang, J.; Phelan, P. Measurements of nanofluid viscosity and its implications for thermal applications. *Appl. Phys. Lett.* **2006**, *89*, 133108. [[CrossRef](#)]
102. Mouromtseff, I.E. Water and forced-air cooling of vacuum tubes nonelectronic problems in electronic tubes. *Proc. IRE* **1942**, *30*, 190–205. [[CrossRef](#)]
103. Yang, X.F.; Liu, Z.-H.; Zhao, J. Heat transfer performance of a horizontal micro-grooved heat pipe using CuO nanofluid. *J. Micromech. Microeng.* **2008**, *18*, 035038. [[CrossRef](#)]
104. Khandekar, S.; Joshi, Y.; Mehta, B. Thermal performance of closed two-phase thermosyphon using nanofluids. *Int. J. Therm. Sci.* **2008**, *47*, 659–667. [[CrossRef](#)]
105. Bahiraei, M.; Heshmatian, S. Electronics cooling with nanofluids: A critical review. *Energy Convers. Manag.* **2018**, *172*, 438–456. [[CrossRef](#)]
106. Nazari, M.; Karami, M.; Ashouri, M. Comparing the thermal performance of water, Ethylene Glycol, Alumina and CNT nanofluids in CPU cooling: Experimental study. *Exp. Therm. Fluid Sci.* **2014**, *57*, 371–377. [[CrossRef](#)]
107. Guo, W.; Li, G.; Zheng, Y.; Dong, C. Numerical study of nanofluids thermal and hydraulic characteristics considering Brownian motion effect in micro fin heat sink. *J. Mol. Liq.* **2018**, *264*, 38–47. [[CrossRef](#)]
108. Kahani, M.; Heris, S.Z.; Mousavi, S.M. Comparative study between metal oxide nanopowders on thermal characteristics of nanofluid flow through helical coils. *Powder Technol.* **2013**, *246*, 82–92. [[CrossRef](#)]
109. Vasu, V.; Kumar, K.M. Analysis of nanofluids as cutting fluid in grinding EN-31 steel. *Nano-Micro Lett.* **2011**, *3*, 209–214. [[CrossRef](#)]
110. Najiha, M.S.; Rahman, M.; Yusoff, A.R. Flank Wear Characterization in Aluminum Alloy (6061 T6) With Nanofluid Minimum Quantity Lubrication Environment Using an Uncoated Carbide Tool. *J. Manuf. Sci. Eng.* **2015**, *137*, 061004. [[CrossRef](#)]
111. Sujith, S.V.; Mulik, R.S. Surface Integrity and Flank Wear Response Under Pure Coconut Oil-Al<sub>2</sub>O<sub>3</sub> Nano Minimum Quantity Lubrication Turning of Al-7079/7 wt%-TiC In Situ Metal Matrix Composites. *J. Tribol.* **2022**, *144*, 1–15. [[CrossRef](#)]
112. Sarkar, J.; Ghosh, P.; Adil, A. A review on hybrid nanofluids: Recent research, development and applications. *Renew. Sustain. Energy Rev.* **2015**, *43*, 164–177. [[CrossRef](#)]
113. Asadi, A.; Asadi, M.; Rezaniakolaei, A.; Rosendahl, L.; Afrand, M.; Wongwises, S. Heat transfer efficiency of Al<sub>2</sub>O<sub>3</sub>-MWCNT/thermal oil hybrid nanofluid as a cooling fluid in thermal and energy management applications: An experimental and theoretical investigation. *Int. J. Heat Mass Transf.* **2018**, *117*, 474–486. [[CrossRef](#)]
114. Boubaker, R.; Harmand, S.; Platel, V. Numerical analysis of the impact of nanofluids and vapor grooves design on the performance of capillary evaporators. *Transp. Porous Media* **2018**, *122*, 401–419. [[CrossRef](#)]
115. Sarafraz, M.; Pourmehran, O.; Yang, B.; Arjomandi, M. Assessment of the thermal performance of a thermosyphon heat pipe using zirconia-acetone nanofluids. *Renew. Energy* **2019**, *136*, 884–895. [[CrossRef](#)]
116. Mebarek-Oudina, F. Convective heat transfer of Titania nanofluids of different base fluids in cylindrical annulus with discrete heat source. *Heat Transf. Asian Res.* **2019**, *48*, 135–147. [[CrossRef](#)]
117. Singh, T.; Dureja, J.S.; Dogra, M.; Bhatti, M.S. Environment friendly machining of inconel 625 under nano-fluid minimum quantity lubrication (NMQL). *Int. J. Precis. Eng. Manuf.* **2018**, *19*, 1689–1697. [[CrossRef](#)]
118. Behera, B.C.; Chetan; Setti, D.; Ghosh, S.; Rao, P.V. Spreadability studies of metal working fluids on tool surface and its impact on minimum amount cooling and lubrication turning. *J. Mater. Process. Technol.* **2017**, *244*, 1–16. [[CrossRef](#)]